Journal of Applied Physics

Insights into the fabrication of sub-100 nm textured thermally drawn fibers

Cite as: J. Appl. Phys. **125**, 175301 (2019); https://doi.org/10.1063/1.5089022
Submitted: 16 January 2019 • Accepted: 05 April 2019 • Published Online: 03 May 2019

Tung Nguyen Dang, Inès Richard, Etienne Goy, et al.

Journal of Applied Physics ARTICLE scitation.org/journal/jap

Insights into the fabrication of sub-100 nm textured thermally drawn fibers

Cite as: J. Appl. Phys. **125**, 175301 (2019); doi: 10.1063/1.5089022
Submitted: 16 January 2019 · Accepted: 5 April 2019 ·
Published Online: 3 May 2019

View Online Export Citation CrossMark

Tung Nguyen Dang,[a] Inès Richard,[a] Etienne Goy, Federica Sordo, and Fabien Sorin[b]

AFFILIATIONS

Photonic Materials and Fiber Devices Laboratory, Institute of Materials, Ecole Polytechnique Fédérale de Lausanne, Lausanne CH-1015, Switzerland

[a]**Contributions:** T. N. Dang and I. Richard contributed equally to this work.
[b]**Author to whom correspondence should be addressed:** Fabien.sorin@epfl.ch

ABSTRACT

The preform-to-fiber thermal drawing process has been recently proposed for the fabrication of fibers and microchannels with submicrometer surface textures. To better control the final architecture and reach small feature size down to tens of nanometers however, a proper understanding and modeling of the fluids dynamics at play during the fabrication of the texture is needed. Here, we present an analytical model describing comprehensively the reflow of periodic polymer micropatterns of arbitrary shape in isothermal annealing as well as in a fiber drawing process. Experiments on square-grooved thermoplastic plates subjected to both treatments show excellent agreement with the calculated theoretical values. Based on this model, we could identify a strategy and the corresponding materials to fabricate sub-100 nm surface-patterned fibers. These results deepen the understanding and control of thermal-based approaches for polymer surface texturing and open novel opportunities for textured fibers and microchannels in bioengineering, microfluidics, or smart textiles.

I. INTRODUCTION

High aspect ratio constructs such as thin fibers and microchannels with well-defined surface textures are gaining an increasing technological interest in a wide range of applications including scaffold for nerve regeneration,[1–3] microfluidics, healthcare monitoring, and smart textiles. The fabrication of submicrometer textures onto thin fibers of tens-of-micrometers in diameters, or onto the inner wall of small microchannels, is, however, very challenging even with advanced lithography processes. Recently, the preform-to-fiber thermal drawing technique has been proposed as an ideal, simple, and scalable platform to generate surface-patterned fibers, ribbons, and microchannels.[4–6] Such textures were successfully exploited to tailor surface wetting of textiles without chemical treatment, to concentrate solar energy onto photovoltaic cells, or to enhance nerve guiding effect in regenerative scaffolds.[5–9] The fiber processing technique, initially developed for the fabrication of optical fibers, consists of feeding a macroscale preform made out of amorphous glasses or polymers into a heating furnace that softens the materials so as to draw it into kilometer-long microstructured functional fibers.[4,10–13] To impart texture at the fiber level, a macroscale version is machined onto the preform at the submillimeter scale using milling, laser-cutting, or hot-embossing techniques.[4–7] During the drawing process, the preform elongates into a long fiber, while the cross section feature reduces accordingly, potentially reaching the submicrometer scale. The leveling of the textured surface induced by Laplace pressure, commonly referred to as reflow, sets, however, an ultimate feature size to the achievable structures at the fiber level. This has been shown in previous publications, together with the proposed practical strategies to alleviate this limitation.[5,6] Thus far however, a model describing the reflow of an arbitrary textured shape preform and its systematic comparison with experimental values as reflow evolves over time during drawing has not been proposed. Such detailed understanding of the process remains essential to better characterize reflow and design arbitrary textures that can reach lower feature sizes.

In this letter, we establish a reflow model that can be applied to any periodic texture and demonstrate experimentally its validity during both an isothermal annealing and a thermal drawing experiment. We start with the description and experimental characterization of the isothermal reflow of a texture imprinted on a thick polymer plate, which reveals the contribution of high frequency modes during the early stage of reflow. We use this first analysis to

tackle the problem of deformation during thermal drawing, which combines reflow and monolithic scaling at different temperatures. We compare and show an excellent agreement between our theoretical prediction of reflow and experimental data taken at different positions along the preform-to-fiber region. This enables us to critically discuss several strategies that have been employed to enhance the cross-sectional preservation and show that lowering the reflow driving force holds the key for successful texturing of fibers and microchannels at feature sizes as low as a few tens of nanometers. To illustrate this finding, we demonstrate the fabrication of sub-100 nm structures within a thermally drawn fiber by codrawing two materials of low interfacial tension.

II. REFLOW DURING ISOTHERMAL ANNEALING

We start with the study of the reflow deformation of a polymer surface texture under isothermal annealing. We first restrict our investigation to the case of a one-dimensional periodic pattern [in the x direction, see Fig. 1(a) (top)] with a profile $y(x) = h\cos\left(\frac{2\pi}{\lambda}x\right)$ with a periodicity (λ) and a height (h) significantly smaller than the substrate thickness (d). Upon annealing slightly above its glass transition temperature (T_g), the polymer can be considered as a Newtonian incompressible fluid that flows in a regime of very low Reynolds number as we justify below, since the viscosity strongly dominates (typically, $\eta = 10^5 - 10^8$ Pa s). Moreover, we consider the case where the height of the surface pattern is significantly smaller compared to its periodicity ($h \ll \lambda$), which allows to linearize the Laplace pressure in the normal stress boundary condition between the polymer and air.[14,15] A well-known solution of the velocity (u_x, u_y) field in such a configuration is a periodic function in x that decays exponentially in the bulk (y-direction). Applying the kinematic boundary condition allows to relate u_y with the change of height over time, leading to a simple first-order differential equation $\frac{\partial h}{\partial t} = -\frac{h}{\tau}$, and hence $h(t) = h(0)\exp\left(-\frac{t}{\tau}\right)$ with the characteristic reflow time $\tau = \frac{\eta\lambda}{\pi\gamma}$, with η the viscosity of the polymer and γ its surface tension.[5,16,17]

This solution for a single harmonic can be used to treat the case of an arbitrary periodic texture $y(x)$. Assuming that all patterns are regular functions that verify the Dirichlet conditions, $y(x)$ can be written as the sum of sine and cosine modes, with each mode having a period $\lambda_n = \lambda/n$. Because of the linearization conditions, we applied above (low Reynolds number, and $h \ll \lambda$), the Navier–Stokes equations governing the velocity field as well as the boundary conditions are all linear relations. It is then straightforward to realize that injecting $y(x)$ in these equations will project each harmonic into a set of similar equations as described above for a single harmonic.[14] In other words, each mode will decay with a similar expression $h_n = h_{n0}\exp\left(-\frac{t}{\tau_n}\right)$, where h_{n0} is the nth-Fourier term of the original shape, and $\tau_n = \tau/n$.

To verify experimentally this analysis, we apply our model to a square wave texture as shown in Fig. 1(a) (bottom) with an initial height of h_0. The Fourier transform of such function is well-known to be $y(x) = \frac{4h_0}{\pi}\sum_n \frac{(-1)^n}{(2n+1)}\cos\left(\frac{2\pi(2n+1)}{\lambda}x\right)$. Since each mode $h_n = \frac{4}{\pi}\frac{(-1)^n}{(2n+1)}h_0$ evolves like described above, we have a time evolution of the texture given by $y(x,t) = \frac{4h_0}{\pi}\sum_n\left(\frac{(-1)^n}{(2n+1)}e^{-(2n+1)\frac{t}{\tau}}\right)\times\cos\left(\frac{2\pi(2n+1)}{\lambda}x\right)$. A measurable value that can be simply defined is the height of the structure as it reflows at $x = 0$ [λ], which will have the following evolution:

$$\frac{h(t)}{h_0} = \frac{4h_0}{\pi}\sum_n\left(\frac{(-1)^n}{(2n+1)}e^{-(2n+1)\frac{t}{\tau}}\right). \quad (1)$$

This theoretical description of the amplitude decay was verified with isothermal reflow experiments of microimprinted poly(methyl methacrylate) (PMMA) samples (Plexiglass® from Boedeker). The imprinting and annealing processes are illustrated in Fig. 1(b). We first made two polydimethylsiloxane (PDMS) molds with periodical square patterns of period λ of 20 μm and 40 μm, and height h of 10 μm and 20 μm, respectively. The patterns were transferred to PMMA plates by hot pressing (see the supplementary material for more details) that were subsequently annealed inside an oven at 130 °C ± 2 °C for various durations. The typical cross sections of imprinted samples before and after annealing are shown in Fig. 1(b). The vertical error bar corresponds to the statistical standard deviation of the pattern height measurements (UBM laser profilometer), and the horizontal error bar takes into account the temperature variation during the annealing process (supplementary material). The experimental normalized height $h(t)/h_0$ [left-hand side of Eq. (1)] is reproduced in Fig. 1(c), and the theoretical values [right-hand side of Eq. (1)] are shown by three dashed lines corresponding to the temperature uncertainties in the oven, i.e., one theoretical curve for 128 °C, 130 °C, and 132 °C. We used a surface tension $\gamma = 33$ mN/m at 130 °C[18] and viscosity values taken from measurements performed on PMMA plates (supplementary material). In these experiments, the Reynolds and the capillary numbers were $Re = \frac{\rho U h}{\eta} \approx 10^{-5} \ll 1$ and $Ca = \frac{\eta U}{\gamma} \approx 1$, with $U = \frac{h_0}{\tau} \approx 10^{-5}$ m/s and $h = h_0 \approx 10^{-5}$ m, which justifies our earlier approximation of neglecting the inertial term in the Navier–Stokes equations. We note that our analysis considered $h_0 \ll \lambda$, which is initially not completely satisfied, especially when considering the high order modes. However, the contribution of these modes decays much faster than the first-order ones (as $\tau_n = \tau/n$) and disappear over a time scale negligible compared to the overall process. The excellent agreement between Eq. (1) and experimental data further confirms that our model captures well the overall dynamic of the system despite the linearization approximation.

III. REFLOW DURING THERMAL DRAWING

Let us now exploit this first study to tackle the case of the thermal drawing of a pattern on the surface of a preform. The same approximation can be made regarding the incompressibility of the polymer and the low Reynolds number flow during thermal drawing as shown before.[19–21] This time however, as we schematically show in Fig. 2(a), the drawing process entails a non-isothermal reflow with a scaling down of all the cross-sectional geometrical parameters as the fiber is being formed. The periodicity λ of an arbitrary pattern is no longer unchanged during the reflow because of the scaling, h_0 is subjected to reflow and scaling simultaneously, and the surface tension γ and viscosity η are also varying because the temperature varies strongly along the length of the furnace. To model this problem, we can consider the evolution of the surface pattern along an infinitesimal length dz of the preform-to-fiber axis.[5] The overall

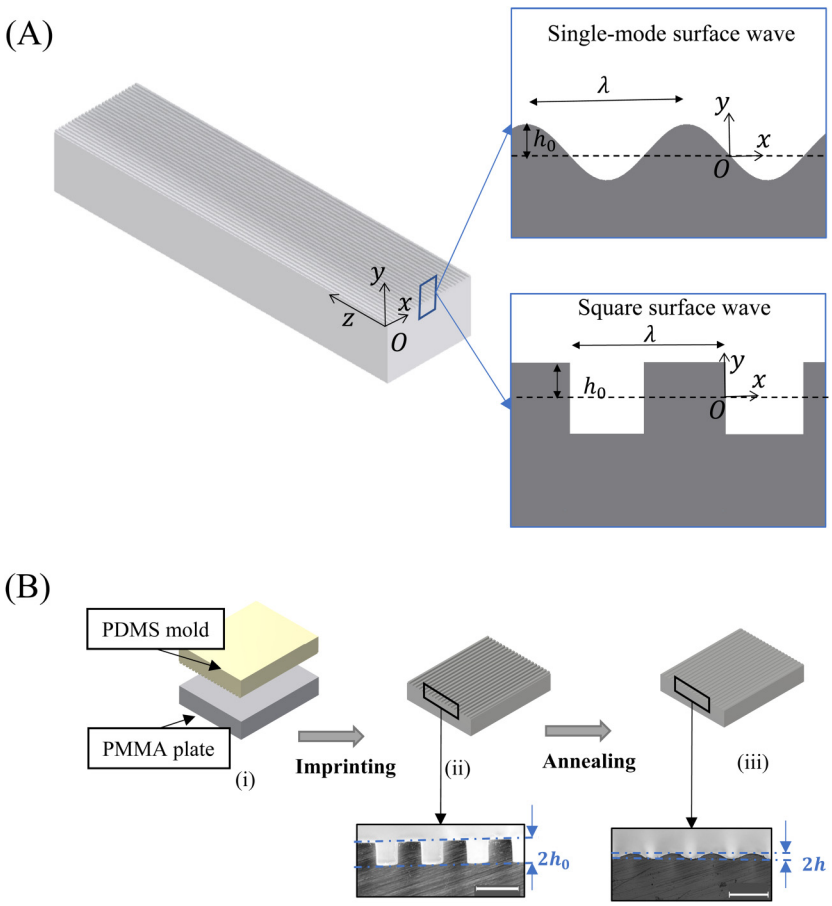

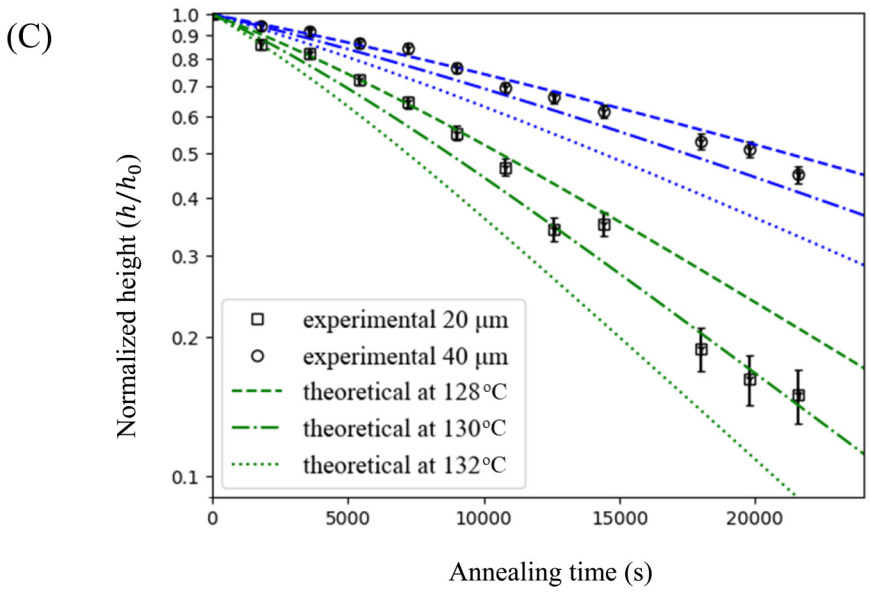

FIG. 1. (a) Schematics of a sinusoidal surface wave and a square surface wave; (b) schematics of the imprinting and annealing experiments and the cross section of a sample after each step. (c) Theoretical (lines) and experimental decay (square and circular dots) of the normalized amplitude of an annealed square surface as function of annealing time. The blue and green lines modes the 20 and 40 micrometer structures, respectively.

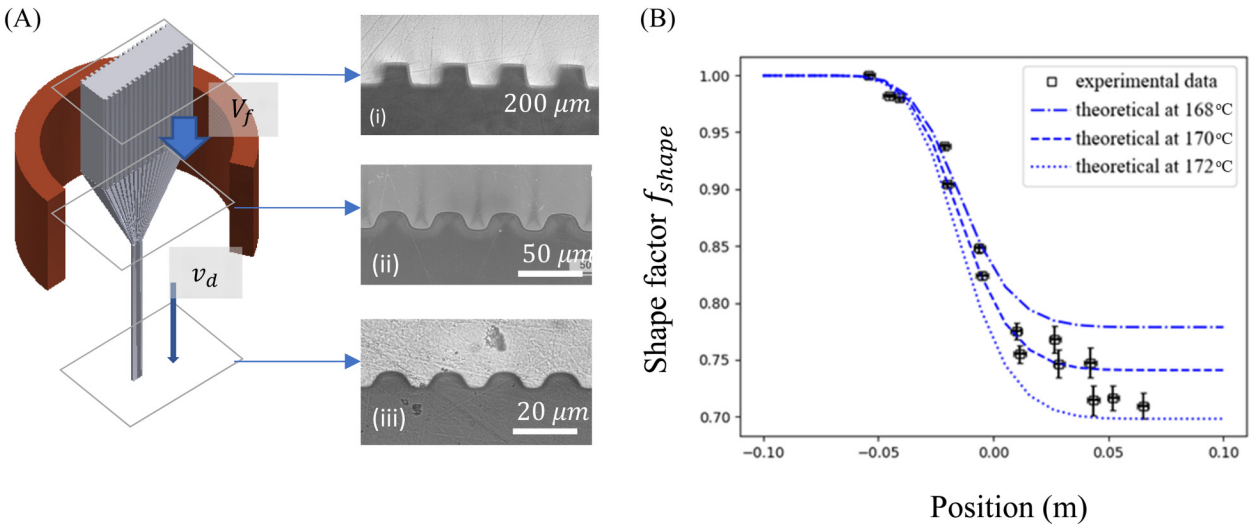

FIG. 2. (a) Schematics of the drawing process with a-(i)–(iii) micrographs of the cross-sectional cut at different positions from the preform to the fiber. (b) The experimental and theoretical shape factor along the drawing direction. The lines correspond to the calculated value of the shape factor with $T_0 = 168\,^{\circ}\mathrm{C}$, $170\,^{\circ}\mathrm{C}$, and $172\,^{\circ}\mathrm{C}$, respectively.

change of height results from the sum of two types of deformation, the scaling deformation $dh_{sc}(z)$ coming from the drawing process and the thermal reflow deformation $dh_{re}(z)$. The former results from simple volume conservation and can be expressed as $dh_{sc}(z) = -\frac{1}{2}\frac{h}{v}\,dv$ with $v = v(z)$ being the fluid velocity along the furnace axis considered uniform in the cross section. The latter follows a similar evolution as described above since between z and $z + dz$ we can consider an isothermal reflow at $T(z)$ for a period of $\lambda(z)$, $dh_{re}(z) = -\frac{h}{\tau(z)}\,dt$, with a corresponding time $dt = \frac{dz}{v(z)}$.

This evolution can also be derived for a square pattern using again a spectral approach. The reflow between the positions z and $z + dz$ applies to each mode as explained above. The scaling down is also a uniform transformation that applies to all modes. Hence, we can write for each mode

$$\frac{dh_n}{h_n(z)} = -\frac{1}{2}\frac{dv}{v(z)} - \frac{dz}{v(z) \times \tau_n(z)},$$

which gives for each mode $h_n(z) = \left(\frac{v(z)}{V_f}\right)^{-\frac{1}{2}} \exp\left(\int_{-z_0}^{z} -\frac{1}{v(z)\,\tau_n(z)}dz\right)$, where we fix the center of the furnace at $z = 0$, $-z_0$ represents the top of the furnace, and V_f is the preform feeding speed.

The expression of the amplitude for a square pattern, following our calculations in Eq. (1), is finally written as

$$h(z) = \frac{4h_0}{\pi}\left(\frac{v(z)}{V_f}\right)^{-\frac{1}{2}} \sum_n \frac{(-1)^n}{(2n+1)} \exp\left(\int_{-z_0}^{z} -\frac{(2n+1)}{v(z)\,\tau(z)}dz\right). \quad (2)$$

Due to the volume conservation, we can write $\left(\frac{V_f}{v(z)}\right)^{-1/2} = \frac{\lambda_0}{\lambda(z)}$, thus Eq. (2) can be rearranged to define a dimensionless quantity that we name the shape factor f_{shape}

$$f_{shape}(z) = \frac{h(z)}{h_0}\frac{\lambda_0}{\lambda(z)} = \frac{4}{\pi}\sum_n \frac{(-1)^n}{(2n+1)} \exp\left(\int_{-z_0}^{z} -\frac{(2n+1)}{v(z)\,\tau(z)}dz\right). \quad (3)$$

This shape factor is a quantitative measure of the preservation of the structure in a drawing process. It varies from 0 to 1, with $f_{shape} = 1$ corresponding to a perfect preservation of the cross-sectional shape, whereas $f_{shape} = 0$ corresponds to a complete collapse of the structure.

To verify experimentally this analysis, a $200\,\mu$m-square pattern embossed onto a thick PMMA plate was thermally drawn into a fiber as shown in Fig. 2(a), with a feeding (V_f) and a drawing speed (v_d) fixed at 1 mm/min and 100 mm/min, respectively. To evaluate the shape factor according to our analysis [the right-hand side of Eq. (3)] in such an experiment, we must know the material viscosity $\eta(T(z))$ and surface tension $\gamma(T(z))$, as well as the drawing speed $v(z)$, at all z positions. First, we show in the supplementary material that the expression of $v(z)$ is given by $v(z) = \exp\left(\ln V_f + \frac{\int_0^z \frac{dz}{\eta(z)}}{\int_0^L \frac{dz}{\eta(z)}}\frac{v_d}{V_f}\right)$. To evaluate the viscosity as a function of z, the temperature distribution inside the furnace is needed. We measured it at different points along the furnace axis with a thermocouple, and the collected data fitted a quadratic profile $T(z) = T_0 - a \times z^2$, with $T_0 = 170 \pm 2\,^{\circ}\mathrm{C}$ and $a = 1.43\,^{\circ}\mathrm{C\,cm^{-2}}$, fixing the center of the furnace at $z = 0$. Knowing the dependence of the viscosity on temperature, we can extract $\eta(z)$, whereas the surface tension of PMMA was taken as $\gamma(T) = 41.1 - 0.078 \times T(^{\circ}\mathrm{C})$[18] (supplementary material). The theoretical value

obtained is shown as a dash line in Fig. 2(b), with the uncertainty represented by two dotted lines. The large uncertainty in the model results from the difficulty to measure accurately the temperature inside the furnace. Even taking a conservative uncertainty of $\pm 2\,^{\circ}\mathrm{C}$ for the measured temperature, the induced variation of viscosity leads to an uncertainty of around 10%.

To confront this theoretical value to experimental data, we now must measure experimentally the evolution of the parameter $\frac{h(z)}{h_0}\frac{\lambda_0}{\lambda(z)}$ during the draw. To do so, we stopped feeding and drawing simultaneously when the drawing process became steady and removed the preform-to-fiber construct from the furnace. We then cut and polished the exposed cross section at several positions along the z-axis (using SiC papers Struer P4000). Figure 2(a) shows three examples of the preform-to-fiber cross sections at the preform level, at the necking-down region, and at the fiber level, respectively. We could then image with an optical microscope (Leika DM 2700 M) these cross sections and measure the height of the structure $h(z)$ and its period $\lambda(z)$ to obtain the shape factor at different positions. The experimental data are plotted in Fig. 2(b) and compared with the theoretical value described above, with a very good agreement observed. The vertical and horizontal error bars correspond to the statistical standard deviation of the height measurement of the patterns and the distance measurement of each cut to the top of the preform, respectively (supplementary material). Since our model now accounts for the evolution of the pattern during the entire fiber drawing process, in contrary to previous work that only assessed the final shape at the fiber level, it constitutes an interesting tool to better understand reflow during fiber processing and propose strategies to keep f_{shape} with a value close to 1.

IV. DISCUSSION

From Eq. (3), we see that one way to do so is to make τ as high as possible, as $f_{shape} \underset{\tau\to\infty}{\to} 1$. For that purpose, for a targeted pattern size λ at the fiber level, one can either increase the viscosity η or decrease the surface tension γ of the drawn materials. The former route was exploited for example by using high-mechanical-strength polymers, such as polyetherimide (PEI), which led to the fabrication of textured fibers with feature size as small as 20 μm.[7,9] Reducing the temperature of the preform surface during drawing to locally lower the viscosity at the texture level was also used to reach submicrometer feature sizes.[6] An alternating approach consists in decreasing the surface tension contribution by interfacing the patterned surface of a preform with another polymer during drawing. As a result, the driving force of the thermal reflow deformation becomes the interfacial tension between the two polymers, which can be chosen to be much smaller than the surface tension of either component. It was previously shown that a square pattern with 300 nm feature size could be obtained by thermally drawing a multi-material polycarbonate (PC)/polyethylene (PE) fiber. Contrary to a PC-only fiber, the PC/PE could maintain the structure because the interfacial tension between the two polymers (6.9 mN/m at 20 °C) is more than 5 times lower than between the PC and air.[18,22] With the model developed above, we can precisely anticipate what would be the reflow factor for a square pattern of PC and PC/PE. It appears that while the PC/PE system enables to maintain a shape factor close to 1 for a 300-nm-feature-sized pattern (the feature size is defined as half of the period, corresponding to the width of an individual groove), it decreases quickly to 0 when feature size gets to sub-100 nm region. An alternative pair of polymers to maintain feature sized down to 100 nm at the fiber level is PC/PMMA. These materials can be codrawn and have an estimated surface tension of 0.39 mN/m (supplementary material), more than an order of magnitude below the one of PC and PE. For such a value, the shape factor remains close to 1 at 100 nm feature size, which makes it possible to reach such a small scale at the fiber level (supplementary material). To verify experimentally this analysis, we fabricated a cylindrical preform with a textured PC core surrounded by a PMMA cladding that we drew a first time to obtain a submillimeter scale fiber as shown in Fig. 3(a). We then assembled several of these fibers and drew them a second and third time to reach sub-100 nm features. In Figs. 3(b) and 3(c) we show cross sections after the second and third draw, respectively. PMMA was etched by dipping the fibers into acetic acid to expose the PC free surfaces. While imaging at this scale is challenging, the SEM micrographs of Fig. 3(c) reveal patterned fibers drawn with submicrometer diameter, on which textures are maintained with feature sizes well below 100 nm, around 20–30 nm in terms of height as can be seen in Fig. 3(c)-iii.

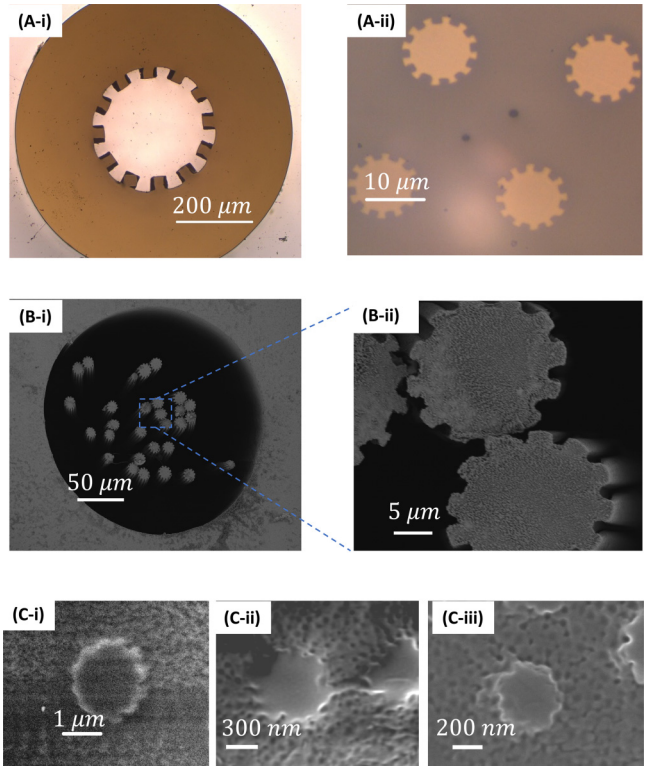

FIG. 3. (a-i) and (a-ii) Micrographs of the once-draw and twice-draw PC textured fibers covered by PMMA cladding, respectively, (b) the twice-drawn fiber after dissolution of PMMA, (c) thrice-drawn fibers with sub-100 nm feature size at different draw-down ratios.

While the agreement we achieved is very good, our model still involves some assumptions that could be alleviated in future research. Numerical solutions could be developed in order to take into account the nonlinearity of the Laplace pressure for patterns with a height larger than the periodicity ($h < \lambda$). In addition, our model could be extended to non-Newtonian fluid and the coupling between the thermal reflow and drawing scaling could also be considered to refine the model, particularly for materials with a strong non-Newtonian behavior.

V. CONCLUSION

In conclusion, we presented an in-depth theoretical and experimental study of the thermal reflow deformation of polymer surfaces in isothermal and in thermal drawing conditions. Analytical descriptions of the deformation of a square wave were obtained and showed very good agreement with the experimental data. We showed that by decreasing the driving force of the reflow, we could keep the sharpness of the structure at a micrometer scale and achieved sub-100 nm patterned fibers. The simplicity of our model can be applied to multiple fiber shapes and periodic structures, allowing for a variety of configurations to be engineered. This paves the way towards the design of advanced fibers for novel applications in optical waveguides, bioengineering, microfluidics, or deformation sensing.[4,10,13,23,24] Beyond thermal drawing, the theoretical framework presented herein could find an interest in other processes such as for fiber spinning techniques or microlens fabrication.

SUPPLEMENTARY MATERIAL

See the supplementary material that accompanies this paper for details about sample fabrication and characterization, analytical expression of velocity profile along the drawing direction, error bar estimation, and calculation of shape factor depending on final feature sizes on fibers.

ACKNOWLEDGMENTS

The authors are grateful to Professor Veronique Michaud and Dr. Stefano Mischler for the use of equipment in their lab for the characterization of materials and fibers. The authors also would like to acknowledge the Swiss National Science Foundation (NSF, CH) (Grant No. 200021_169650), the Swiss Competence Center for Materials Science and Technology (CCMX) challenge funding scheme, and the European Research Council (ERC) (Starting Grant No. 679211 "FLOWTONICS") for their funding support.

REFERENCES

[1]W. Zeng *et al.*, "Fiber-based wearable electronics: A review of materials, fabrication, devices, and applications," Adv. Mater. **26**, 5310–5336 (2014).
[2]H. Sun, Y. Zhang, J. Zhang, X. Sun, and H. Peng, "Energy harvesting and storage in 1D devices," Nat. Rev. Mater. **2**, 17023 (2017).
[3]W. Daly, L. Yao, D. Zeugolis, A. Windebank, and A. Pandit, "A biomaterials approach to peripheral nerve regeneration: Bridging the peripheral nerve gap and enhancing functional recovery," J. R. Soc. Interf. **9**, 202–221 (2012).
[4]W. Yan *et al.*, "Advanced multimaterial electronic and optoelectronic fibers and textiles," Adv. Mater. **31**, 1802348 (2018).
[5]T. Nguyen-Dang *et al.*, "Controlled sub-micrometer hierarchical textures engineered in polymeric fibers and microchannels via thermal drawing," Adv. Funct. Mater. **27**, 1605935 (2017).
[6]T. Khudiyev, C. Hou, A. M. Stolyarov, and Y. Fink, "Sub-micrometer surface-patterned ribbon fibers and textiles," Adv. Mater. **29**, 1605868 (2017).
[7]A. Yildirim, M. Yunusa, F. E. Ozturk, M. Kanik, and M. Bayindir, "Surface textured polymer fibers for microfluidics," Adv. Funct. Mater. **24**, 4569–4576 (2014).
[8]E.-H. Banaei and A. F. Abouraddy, "Design of a polymer optical fiber luminescent solar concentrator," Prog. Photovoltaics Res. Appl. **23**, 403–416 (2015).
[9]R. A. Koppes *et al.*, "Thermally drawn fibers as nerve guidance scaffolds," Biomaterials **81**, 27–35 (2016).
[10]M. A. Schmidt, A. Argyros, and F. Sorin, "Hybrid optical fibers – An innovative platform for in-fiber photonic devices," Adv. Opt. Mater. **4**, 13–36 (2016).
[11]M. Bayindir, A. F. Abouraddy, F. Sorin, J. D. Joannopoulos, and Y. Fink, Opt. Photonics News **15**, 24 (2004).
[12]F. Sorin, G. Lestoquoy, S. Danto, J. D. Joannopoulos, and Y. Fink, "Resolving optical illumination distributions along an axially symmetric photodetecting fiber," Opt. Express **18**, 24264 (2010).
[13]W. Yan *et al.*, "Semiconducting nanowire-based optoelectronic fibers," Adv. Mater. **29**, 1700681 (2017).
[14]L. G. Leal, *Advanced Transport Phenomena: Fluid Mechanics and Convective Transport Processes* (Cambridge University Press, 2007).
[15]T. Leveder, S. Landis, and L. Davoust, "Reflow dynamics of thin patterned viscous films," Appl. Phys. Lett. **92**, 90–93 (2008).
[16]M. Hamdorf and D. Johannsmann, "Surface-rheological measurements on glass forming polymers based on the surface tension driven decay of imprinted corrugation gratings," J. Chem. Phys. **112**, 4262 (2000).
[17]M. L. Henle and A. J. Levine, "Capillary wave dynamics on supported viscoelastic films: Single and double layers," Phys. Rev. E **75**, 021604 (2007).
[18]J. E. Mark, *Physical Properties of Polymers Handbook. Physical Properties of Polymers Handbook* (Springer-Verlag, New York, 2007).
[19]S. C. Xue *et al.*, "Role of material properties and drawing conditions in the fabrication of microstructured optical fibers," J. Light. Technol. **24**, 853–860 (2006).
[20]S. S. C. Xue *et al.*, "Fabrication of microstructured optical fibers-part I: Problem formulation and numerical modeling of transient draw process," J. Light. Technol. **23**, 2245–2254 (2005).
[21]E. Pone *et al.*, "Drawing of the hollow all-polymer Bragg fibers," Opt. Express **14**, 5838–5852 (2006).
[22]S. Wu, *Polymer Interface and Adhesion* (Dekker, New York, 1982).
[23]T. Nguyen-Dang *et al.*, "Multi-material micro-electromechanical fibers with bendable functional domains," J. Phys. D Appl. Phys. **50**, 144001 (2017).
[24]T. Khudiyev *et al.*, "Electrostrictive microelectromechanical fibres and textiles," Nat. Commun. **8**, 1435 (2017).